JOURNAL OF SOLID STATE CHEMISTRY **134,** 110–119 (1997)
ARTICLE NO. SC977549

A Powder Neutron Diffraction Study of Structure and Magnetism in $NiCr_2S_4$

Anthony V. Powell,*,[1] Douglas C. Colgan,* and Clemens Ritter†

*Department of Chemistry, Heriot-Watt University, Riccarton, Edinburgh EH14 4AS, United Kingdom; and †Institut Max von Laue–Paul Langevin, F-38042 Grenoble, France

Received March 24, 1997; accepted July 15, 1997

Powder neutron diffraction data for $NiCr_2S_4$ have been collected over the temperature range $1.8 \leq T \leq 286$ K. The Cr_3S_4 structure (space group $I2/m$) is adopted at all temperatures. Refinement of 286 K data ($a = 5.8954(14)$ Å, $b = 3.4066(8)$ Å, $c = 11.0589(22)$ Å, $\beta = 91.362(4)°$) demonstrates that the distribution of nickel and chromium cations between sites in a fully occupied metal layer and sites in an ordered vacancy layer is close to that expected for the normal structure type. Data collected at 1.8 K ($a = 5.8621(5)$ Å, $b = 3.4051(2)$ Å, $c = 11.0297(9)$ Å, $\beta = 91.607(6)°$) reveal the presence of long-range magnetic order, involving a doubling of the unit cell in both the a and c directions. Cations in the fully occupied metal layer possess an ordered magnetic moment of 1.57(6) μ_B which is directed parallel to the cation layers. Cations in the vacancy layer have a moment of 1.36(8) μ_B which is directed toward the anion layers. The magnetic ordering temperature was determined as 180(5) K. These results are correlated with magnetic susceptibility and electrical conductivity data. © 1997 Academic Press

INTRODUCTION

Many binary chalcogenides of stoichiometry M_3X_4 adopt the Cr_3S_4 structure (Fig. 1), which is an ordered defect structure intermediate between the NiAs and CdI_2 types (1). In the latter structure, cations occupy octahedral sites between alternate pairs of hexagonally close-packed anion layers. The resulting stacking sequence may be represented schematically as $XMXXMX$. In the Cr_3S_4 structure, additional cations occupy, in an ordered manner, half of the remaining vacant octahedral sites, resulting in an $XMXM_{0.5}XMX$ stacking sequence. Two crystallographically distinct cation sites can therefore be identified as indicated by the alternative formulation $(M)[M_2]S_4$, where (M) and $[M]$ represent cations in the vacancy and fully occupied layers, respectively. For a ternary sulfide $M'M_2S_4$, two extreme cation arrangements are possible corresponding to the normal $(M')[M_2]S_4$ and inverse $(M)[M'M]S_4$ structure types (2). We are currently investigating ternary sulfides of the Cr_3S_4 structure type in an effort to modify systematically electronic and magnetic properties by chemical substitution. Initial studies have focused on the system $V_xCr_{3-x}S_4$ $(0.0 \leq x \leq 1.0)$ for which compositionally induced changes in structural, electronic, and magnetic properties have been observed. A combination of X-ray and neutron scattering has shown (3) that there is a change in relative site preferences of the cations associated with anomalies in the cell parameter vs. composition curves. These may be correlated with changes in magnetic and electronic properties (4) (spin-glass → antiferromagnet; semiconductor → metal) observed with decreasing vanadium content. In the stoichiometric phase VCr_2S_4, vanadium is equally distributed between the two available sites (5), contrary to the previously accepted view that the structure is of the normal type (2). This distribution persists with decreasing vanadium content until at $x \approx 0.2$ the structure approaches the normal type, with over 90% of vanadium occupying sites in the vacancy layer (3).

In seeking to extend these studies, we have recently prepared the series $Ni_xCr_{3-x}S_4$ (6) in which Cr(II) is progressively substituted by Ni(II), the d^{n+5} analogue of V(II). Solid solution behavior is found throughout the series and physical properties differ significantly from those of the analogous vanadium-containing series; in particular, delocalized electron behavior persists over a much wider range of composition. The end-member phase $NiCr_2S_4$, first reported by Jellinek (7), has been investigated by several groups. Bouchard and Wold (8) have argued, on the basis of resistivity and Seebeck coefficient measurements, that $NiCr_2S_4$ is a low-activation-energy semiconductor whose electrical properties are intermediate between those of typical metals and semiconductors. Semiconducting behavior is consistent with the schematic energy-level diagrams presented by Holt *et al.* (9), who assumed the structure to be of the normal type. A powder neutron diffraction study (10) carried out at 4.2 K demonstrated that the compound orders antiferromagnetically at low temperatures, although the Néel temperature was not established. The magnetic structure

[1]To whom correspondence should be addressed.

0022-4596/97 $25.00

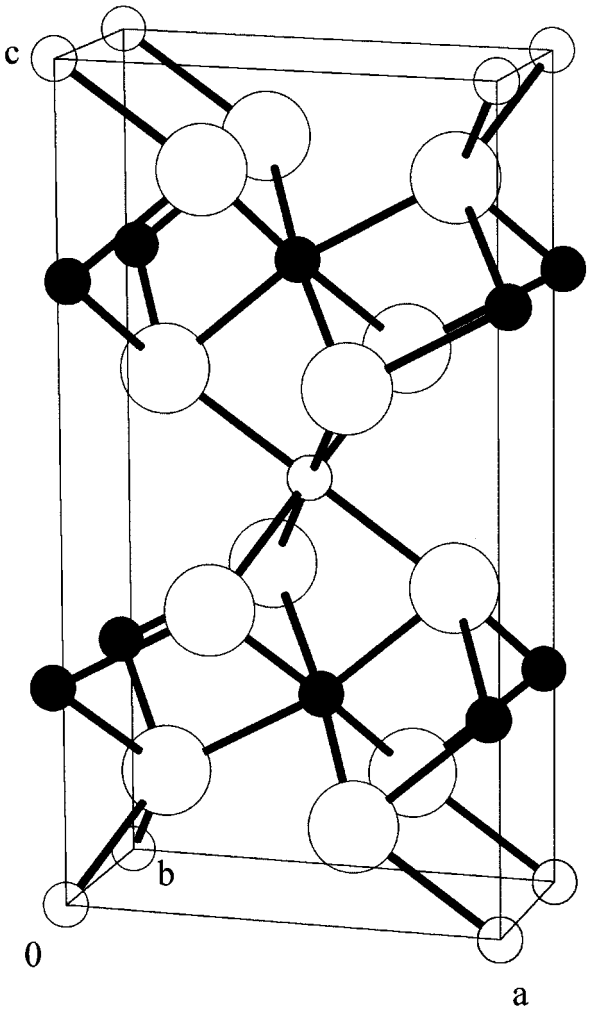

FIG. 1. A ball-and-stick representation of the Cr_3S_4 structure. Large open circles represent anions, small filled circles represent cations in the fully occupied layer, and small open circles represent cations in the vacancy layer.

determined from an integrated intensity analysis of the diffraction data has a propagation vector of $(1/2, 0, \overline{1/2})$ with magnetic moments significantly reduced from their spin-only values. Magnetic susceptibility data (11) show a broad maximum around 210 K, above which the susceptibility is virtually temperature independent and below which the susceptibility rises after passing through a minimum at 100 K. Tressler and Stubican (12) have suggested that this rise corresponds to the onset of ferromagnetic ordering. In connection with our study of the nonstoichiometric $Ni_xCr_{3-x}S_4$ phases, we have investigated the end member, $NiCr_2S_4$, using a combination of techniques and here present the results of magnetic susceptibility, electrical resistivity, and neutron scattering measurements. The latter have enabled the low-temperature magnetic structure and its evolution with temperature to be studied. The structure so determined shows differences from that originally proposed.

EXPERIMENTAL

A mixture of high-purity nickel, chromium, and sulfur powders of nominal stoichiometry $NiCr_2S_{3.93}$ was ground in an agate mortar. A slight deficiency of sulfur was used in light of previous observations by ourselves (4) and others (7) that the phase range of the Cr_3S_4 structure does not extend to the fully stoichiometric composition. The mixture was sealed into an evacuated silica ampoule and fired at a temperature of 1223 K for 24 h. Following regrinding, the sample was fired at 1273 K for two successive 3-day periods with one intermediate regrinding. After the final firing, the product was cooled to 773 K over a period of several hours prior to removal from the furnace.

Reaction progress was monitored by powder X-ray diffraction using a Philips PA2000 powder diffractometer with nickel-filtered Cu$K\alpha$ radiation. The nickel and chromium content of the sample was determined by atomic absorption spectroscopy with a Pye Unicam SP9 spectrophotometer. The sulfur content was determined thermogravimetrically by oxidation in a flow of dry oxygen on a Stanton Redcroft STA-780 thermobalance. Energy-dispersive microanalysis was used both to determine the Ni : Cr ratio and to provide information on sample homogeneity. Data were collected with a JEOL 200FX electron microscope fitted with a Tracor Northern analysis system. A sample of $NiCr_2O_4$ prepared by a precursor route (13) was used as the intensity standard.

Magnetic susceptibility measurements on powdered samples were made using a Quantum Design MPMS2 SQUID susceptometer. Samples were loaded into gelatin capsules at room temperature and data were collected over the temperature range $3 \leq T \leq 296$ K both after cooling the sample in zero applied field (zfc) and after cooling in the measuring field (fc) of 1 kG. Data were corrected for the diamagnetism of the gelatin capsule and for intrinsic core diamagnetism. The electrical resistance of the sample was measured using the four-probe DC technique. An ingot ($\sim 6 \times 3 \times 1$ mm) was cut from a sintered pellet, four 50-μm silver wires were attached using colloidal silver paint, and connections were made to a HP34401A multimeter. Measurements over the temperature range $80 \leq T \leq 400$ K were made by placing the sample in an Oxford Instruments CF1200 cryostat connected to an ITC502 temperature controller.

Powder neutron diffraction data were collected over the angular range $5.05 \leq 2\theta \leq 84.85°$ with a neutron wavelength of 2.524 Å on the D1B diffractometer at the high-flux reactor, ILL, Grenoble. The sample (ca. 2 g) was contained in a thin-walled vanadium can which was mounted in a standard ILL orange cryostat. Data collection times of 3 h were used at 1.8 and 286 K. Variable-temperature

TABLE 1
Analytical Data for $NiCr_2S_4$

Nominal composition	$NiCr_2S_{3.93}$
Nominal Ni : Cr	0.5
Experimentally determined Ni : Cr	0.51(3)
Experimentally determined S : (Ni + Cr)	1.30(1)
Experimentally determined composition	$Ni_{1.01}Cr_{1.99}S_{3.91}$
Ni content (%): observed {calculated}	19.8(5) {20.6}
Cr content (%): observed {calculated}	35.0(5) {35.9}

measurements were made over the range $1.8 \leq T \leq 286$ K by collecting diffraction patterns over 10 min in approximately 8 K temperature increments. Rietveld refinements were carried out using the GSAS package (14) installed on the Heriot-Watt University Alpha 2100-4275 system.

RESULTS

The results of the analysis of chemical composition are shown in Table 1. The experimentally determined composition is in excellent agreement with the stoichiometry of the initial reaction mixture, consistent with the formation of a single-phase product. Furthermore, the Ni : Cr ratio determined by energy-dispersive X-ray microanalysis showed little variation throughout the sample, indicating that a homogeneous product phase had been produced. Powder X-ray diffraction data were indexed on the basis of a monoclinic unit cell and yielded cell parameters similar to those previously determined for Cr_3S_4 (3).

Magnetic susceptibility data (Fig. 2) reveal that zfc and fc curves overlie each other completely, over almost the entire range of temperature studied; a slight divergence is observed only below ca. 60 K. The general form of the curve is similar to that previously obtained by Morris *et al.* (11). Data in the temperature range $200 \leq T \leq 300$ K show an almost constant measured susceptibility. Below 200 K, the susceptibility falls slightly, reaching its minimum at 130 K before increasing on further cooling. Data in the high-temperature region could not be fitted using a Curie–Weiss law, even after inclusion of a temperature-independent term. This, together with the weak temperature dependence of the susceptibility, suggests that a localized-electron description is not applicable to the valence electrons in $NiCr_2S_4$.

Further support for the inapplicability of a localized electron description is provided by a measured resistivity of 0.05 Ω cm at room temperature which is independent of temperature above 300 K (Fig. 3a). On cooling below 300 K, the resistivity begins to increase and continues to do so

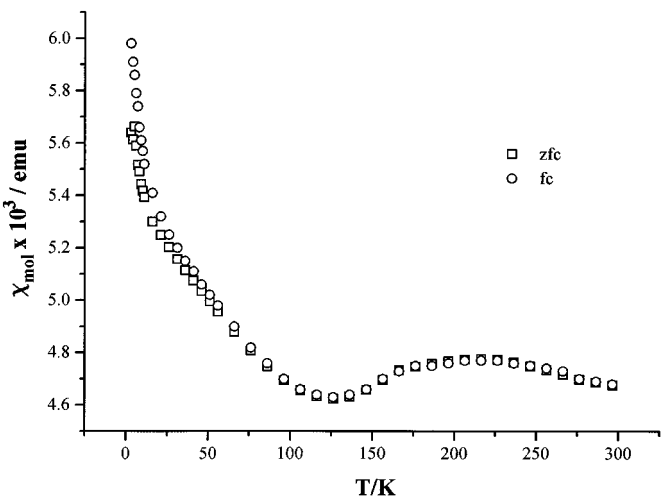

FIG. 2. Zero-field-cooled (zfc) and field-cooled (fc) molar magnetic susceptibilities for $NiCr_2S_4$ measured in a field of 1000 G.

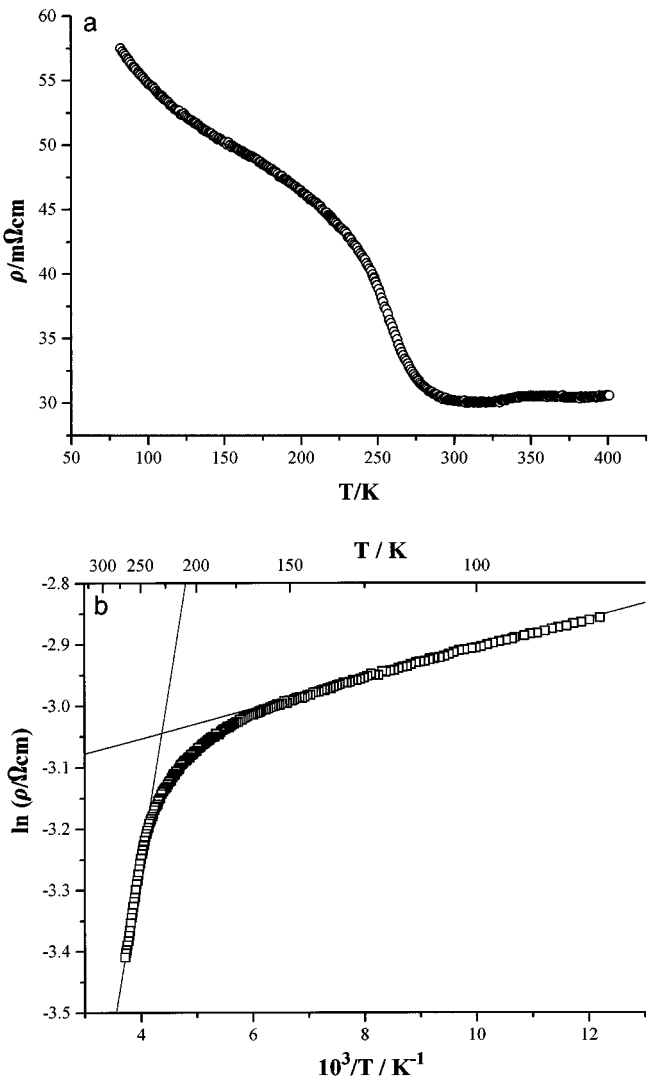

FIG. 3. Electrical data for $NiCr_2S_4$: (a) resistivity as a function of temperature; (b) Arrhenius plot showing the linear fits to data in the high- and low-temperature regions.

down to the lowest temperature studied (80 K). The magnitude of $d\ln(\rho)/dT$ decreases around 200 K. Analysis of data in the temperature range $80 \leq T \leq 300$ K in terms of simple Arrhenius-type behavior (Fig. 3b) reveals two distinct regions. Above 245 K, a linear fit yields an activation energy of $4.8(5) \times 10^{-2}$ eV, whereas below 160 K, an activation energy of $2.12(2) \times 10^{-3}$ eV is obtained. Between these two temperatures, transitional behavior is observed.

Refinement of 286 K Neutron Data

Powder neutron diffraction data over the angular range $20 \leq 2\theta \leq 85^\circ$ were used in the Rietveld refinement, which was initiated in the space group $I2/m$ using lattice parameters determined from the X-ray data. A structural model in which sites in the vacancy and fully occupied layers were occupied exclusively by nickel and chromium, respectively, was used initially. Atomic parameters were taken from our previous investigation of Cr_3S_4 (3) and the neutron scattering lengths incorporated within GSAS were used. The background was fitted using a cosine Fourier series with the coefficients included as refinable parameters. Diffraction peaks were modeled using a pseudo-Voigt peak shape. Refinement of a scale factor, background terms, zero point, and lattice parameters proceeded smoothly. At this stage, a region centered at ca. $2\theta = 72^\circ$ was excluded from the refinement owing to the occurrence of a peak due to vanadium which was instrumental in origin. Refinement of peak shape and thermal parameters followed and resulted in a low weighted residual. Introduction into the refinement of site occupancy factors associated with the cations, with the constraint that overall stoichiometry be maintained, led to a further reduction in the weighted residuals. Introduction of site occupancy factors associated with sulfur did not lead to any significant deviation of their values from unity and they were subsequently fixed at this value. Final observed, calculated, and difference profiles are given in Fig. 4. The corresponding refined parameters appear in Table 2 and important bond lengths and angles can be found in Table 3.

Refinement of 1.8 K Neutron Data

A number of additional reflections were immediately apparent in the powder neutron diffraction pattern collected at 1.8 K. These additional reflections are consistent with a doubling of the unit cell in both the a and c directions with a corresponding propagation vector $(1/2, 0, \overline{1/2})$ as proposed by Andron and Bertaut (10). The crystallographic structure determined at 286 K was used for the structural model at 1.8 K. With the exception of the site occupancy factors, which were fixed at the values determined at 286 K, all of the aforementioned parameters were initially refined. In addition to the region of the profile in which a peak due to vanadium was observed, two further regions, corresponding to instrumental noise ($2\theta \approx 33^\circ$) and a trace of Cr_2O_3 ($2\theta \approx 40^\circ$), were excluded from the refinement. The free-ion form factors (15) for Ni^{2+} and Cr^{3+} were used to describe the angular dependence of the magnetic scattering. The appropriate form factor of the majority species was used to model the average scattering from each of the two crystallographically independent sites. The magnetic structure determined by Andron and Bertaut (10) was used as a starting model. Initially all three magnetic vector components at each of the two sites were allowed to vary. The y component associated with cations in the vacancy layer and the z component associated with cations in the fully occupied layer

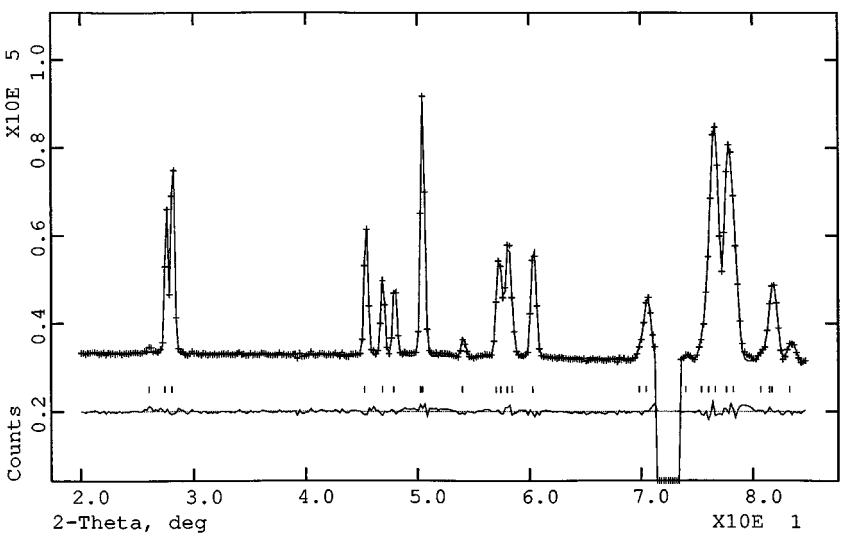

FIG. 4. Final observed (crosses), calculated (full line), and difference (lower full line) neutron profiles for $NiCr_2S_4$ at 286 K. Reflection positions are marked.

TABLE 2
Refined Parameters for $NiCr_2S_4$

(a) $T = 286$ K
Space group: $I2/m$; $a = 5.8954(14)$ Å, $b = 3.4066(8)$ Å, $c = 11.0589(22)$ Å, $\beta = 91.362(4)^\circ$

Atom	Site	x	y	z	B (Å^2)	Occupancy
Ni(1)	2(*a*)	0.0	0.0	0.0	0.6(3)	0.846(14)
Cr(1)	2(*a*)	0.0	0.0	0.0	0.6(3)	0.154(14)
Ni(2)	4(*i*)	− 0.0211(6)	0.0	0.2608(4)	1.0(5)	0.077(7)
Cr(2)	4(*i*)	− 0.0211(6)	0.0	0.2608(4)	1.0(5)	0.923(7)
S(1)	4(*i*)	0.3404(14)	0.0	0.3658(6)	0.4(2)	1.0
S(2)	4(*i*)	0.3307(14)	0.0	0.8797(6)	1.0(2)	1.0

$R_{wp} = 1.3\%$

(b) $T = 1.8$ K
Space group: $I2/m$; $a = 5.8621(5)$ Å, $b = 3.4051(2)$ Å, $c = 11.0297(9)$ Å, $\beta = 91.607(6)^\circ$

						Magnetic vector components			
Atom	Site	x	y	z	B (Å^2)	M_x	M_y	M_z	Moment (μ_B)
$M(1)^a$	2(*a*)	0.0	0.0	0.0	− 0.2(4)	0.94(7)	0.0	− 0.99(8)	1.36(8)
$M(2)^b$	4(*i*)	− 0.0224(9)	0.0	0.2607(5)	0.9(3)	− 1.52(6)	− 0.4(1)	0.0	1.57(6)
S(1)	4(*i*)	0.3404(18)	0.0	0.3657(9)	1.3(4)				
S(2)	4(*i*)	0.3277(18)	0.0	0.8806(8)	− 0.4(4)				

$R_p = 1.6\%$

[a] $M(1)$: 84.6% Ni; 15.4% Cr.
[b] $M(2)$: 7.7% Ni; 92.3% Cr.

refined to values close to zero, the value at which they were subsequently fixed. Final observed, calculated, and difference profiles are given in Fig. 5. Table 2 lists the corresponding refined parameters, and important bond lengths and angles appear in Table 3.

Variable-Temperature Neutron Diffraction Data

Powder neutron diffraction data in the angular range $20 \leq 2\theta \leq 50^\circ$, collected at intermediate temperatures, are plotted in Fig. 6, in which the evolution of the magnetic peaks with temperature may be clearly observed. The magnetic ordering temperature was established by plotting the intensity of the magnetic reflections as a function of temperature, leading to an estimate of $T_N = 180(5)$ K, as shown in Fig. 7 for the (1/2,0,3/2) reflection. Sequential Rietveld refinement, performed on patterns over the entire temperature range studied, allowed the variation of unit cell parameters with temperature to be investigated (Fig. 8). Whereas the b parameter is effectively constant with temperature, both the a and c parameters decrease with decreasing temperature, reaching a constant value below ca. 125 K. The monoclinic distortion increases with decreasing temperature until below 100 K, the angle β is effectively constant. In addition, sequential Rietveld refinement allowed the evolution of the ordered magnetic moment, at each of the two sites, to be investigated below the ordering temperature (Fig. 9).

DISCUSSION

Rietveld refinement of powder diffraction data collected at 286 K resulted in all peaks being fitted, with no evidence for any impurity phases. Although low-temperature data did indicate the presence of trace amounts of Cr_2O_3, the level of this impurity is very low, in accord with the results of chemical analysis. The errors on the isotropic temperature factors were somewhat larger than those reported in our previous work on the $V_xCr_{3-x}S_4$ series (3). In particular, at 1.8 K these errors are comparable with the values themselves, which would account for one of the parameters becoming negative. This is likely to be a consequence of the limited Q range of data collected in this work. However, no significant correlations were observed and the correctness of the structures determined is unaffected.

The lattice parameters determined at 286 K are in close agreement with the room temperature parameters previously reported (7). Both the a and c parameters are reduced relative to those of the isostructural materials Cr_3S_4 and VCr_2S_4 (3). This reduction is in accord with respective

TABLE 3
Bond Lengths (Å) and Bond Angles (°) in $NiCr_2S_4$

	286 K	1.8 K
$M(1)$–S(1)	2.434(5) × 4	2.427(6) × 4
$M(1)$–S(2)	2.386(8) × 2	2.359(10) × 2
Mean $M(1)$–S	2.42	2.40
$M(2)$–S(1)	2.402(8)	2.393(9)
	2.463(6) × 2	2.462(7) × 2
$M(2)$–S(2)	2.369(8)	2.340(8)
	2.334(6) × 2	2.342(7) × 2
Mean $M(2)$–S	2.39	2.39
$M(1)$–$M(2)$	2.890(4) × 2	2.882(5) × 2
$M(2)$–$M(2)$	3.196(6) × 2	3.169(11) × 2
	3.635(7) × 2	3.632(11) × 2
S(1)–$M(1)$–S(1)	88.8(2) × 2	89.1(3) × 2
	91.2(2) × 2	90.9(3) × 2
S(1)–$M(1)$–S(2)	88.2(2) × 4	88.0(3) × 4
	91.8(2) × 4	92.0(3) × 4
S(1)–$M(2)$–S(1)	83.3(3) × 2	83.1(3) × 2
	87.5(3)	87.5(3)
S(1)–$M(2)$–S(2)	93.9(3) × 2	94.0(3) × 2
	89.3(2) × 2	89.6(3) × 2
	87.9(2) × 2	87.6(4) × 2
S(2)–$M(2)$–S(2)	94.4(2) × 2	94.8(4) × 2
	93.7(3)	93.3(4)

ionic radii (16) ($r(Ni^{2+}) = 0.69$ Å, $r(Cr^{2+}) = 0.80$ Å, $r(V^{2+}) = 0.79$ Å). Both cation sites lie at the center of distorted octahedra. The cation in the vacancy layer has four long and two short bonds to sulfur with all S–$M(1)$–S angles close to 90°. The environment of the cation site in the fully occupied layer shows more variation in cation–anion separations and bond angles. Mean cation–anion separations of ca. 2.4 Å are consistent with the sums of respective ionic radii (16).

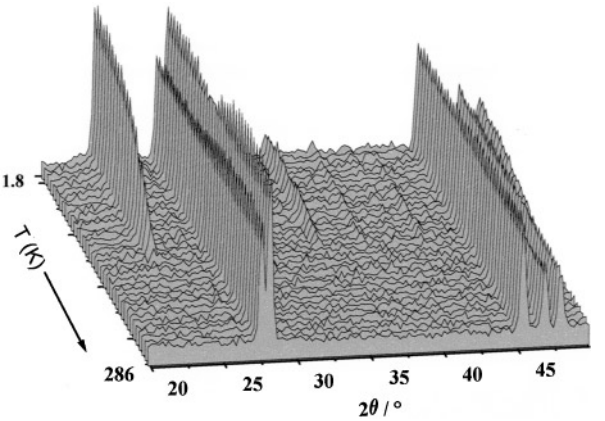

FIG. 6. Powder neutron diffraction data for $NiCr_2S_4$ over the temperature range $1.8 \leq T \leq 286$ K.

The distribution of cations corresponds, in the notation introduced earlier, to $(Ni_{0.846}Cr_{0.154})[Ni_{0.154}Cr_{1.846}]S_4$. This contrasts with the behavior of VCr_2S_4, in which approximately 50% of the divalent ion is found at each of the two cation sites (3). Analysis of the relatively few investigations of cation distributions which have been carried out for ternary Cr_3S_4-type phases (17–19) demonstrates that the preference for sites in the fully occupied layer decreases in the order Ti > V ≈ Cr > Fe. This order reflects the decrease in the critical cation–cation separation (R_c), below which direct overlap of cation orbitals is possible (20). The greater tendency for early transition series cations to delocalize

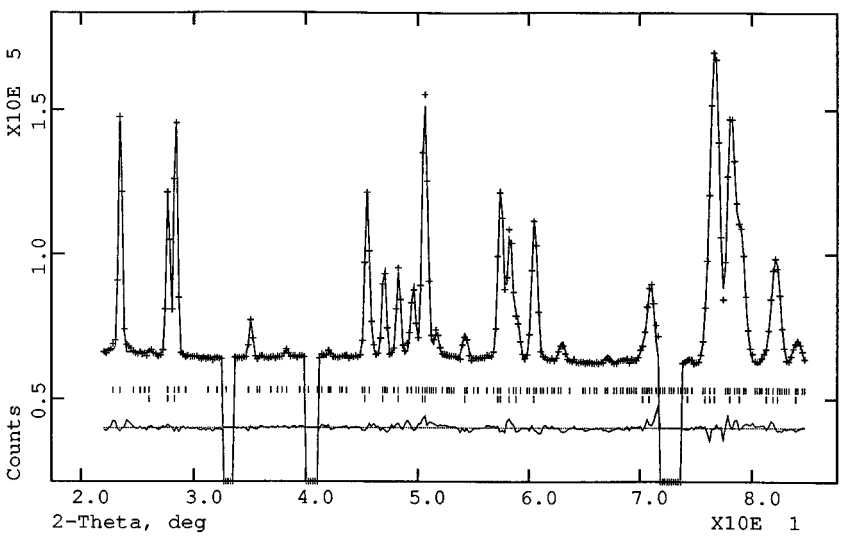

FIG. 5. Final observed (crosses), calculated (full line), and difference (lower full line) neutron profiles for $NiCr_2S_4$ at 1.8 K. Reflection positions are marked: the lower markers refer to the crystallographic unit cell and the upper markers the magnetic unit cell described in the primitive space group $P1$.

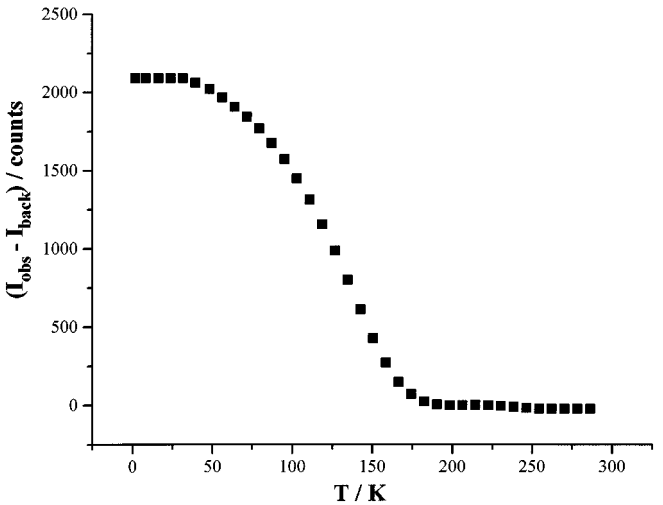

FIG. 7. Temperature variation of the intensity of the (1/2, 0, 3/2) magnetic reflection, where the indices refer to the crystallographic unit cell of $NiCr_2S_4$.

electrons by direct t_{2g}–t_{2g} overlap would favor their occupation of sites in the fully occupied layer. In the case of the $V_xCr_{3-x}S_4$ series, the arrangement adopted is the one which best balances this with the consequent increase in formal negative charge on the $[MS_2]^{n-}$ subunits, which results from the introduction of divalent vanadium at these sites. By contrast, divalent nickel has a much lower tendency to delocalize electrons by t_{2g}–t_{2g} interactions owing to orbital contraction. Consequently, there is no marked preference of Ni(II) for sites in the fully occupied layer and the structure determined in this work appears to continue the aforementioned trend. In particular, the proportion of available nickel (15%) which enters this layer is reduced from that of iron in FeV_2S_4 (25%) (18).

Analysis of the intensity of the magnetic reflections as a function of temperature indicates a magnetic ordering temperature of ca. 180 K. The ordering temperature is reduced from that of $\sim$220 K observed in Cr_3S_4 (21), suggesting that the exchange interactions involving Ni(II) are weaker than those involving Cr(II).

The magnetic structure of $NiCr_2S_4$ has been described (10) in terms of ferromagnetic sheets parallel to the (1 0 $\bar{1}$) planes, which in turn are coupled antiferromagnetically with respect to each other. The same overall features are apparent in the structure determined in this work (Fig. 10). However, there are important differences in the detailed magnetic structure, in particular, the orientation of the moments. In the structure described by Andron and Bertaut (10), all moments, irrespective of cation site, were found to be directed at 45° to the [10$\bar{1}$] direction (corresponding to them lying in the crystallographic *ab* plane) such that the projection of the moment direction on the (10$\bar{1}$) plane made an angle of 122° with the crystallographic *b* axis. In the structure determined here, the orientation of moments at the two crystallographic sites differs markedly. Moments associated with cations in the fully occupied layer ($\mu([M])$) lie in the *ab* plane in an orientation similar to that observed previously. However, those moments associated with sites in the vacancy layer ($\mu((M))$) are oriented such that they lie in the *ac* plane directed at 140° to the [001] direction. This orientation is similar to that of the Cr(II) and Cr(III) moments in Cr_3S_4 whose magnetic structure has been described (22) in terms of ferromagnetic sheets parallel to the (10$\bar{1}$) plane with spins parallel to the [10$\bar{1}$] direction. The complex magnetic structure of $NiCr_2S_4$ may be analyzed in terms of individual superexchange interactions by application of the qualitative rules proposed by Goodenough (23) and Kanamori (24). Interactions within the fully occupied layer are essentially those involving Cr(III) d^3 ions. An analysis similar to that previously applied to Cr_3S_4 (3) predicts that antiferromagnetic and ferromagnetic exchange interactions between cations in the fully occupied layer are simultaneously present. Of the six nearest-neighbor interactions, those of shorter range (3.16 Å) will be dominated by direct cation–cation exchange, resulting in an antiferromagnetic interaction. Conversely, the four longer range interactions will be dominated by correlation superexchange and are predicted to be ferromagnetic. These qualitative arguments are not altered by substitution of ca. 7.5% of Cr(III) in the fully occupied layer with Ni(II). Octahedra in the vacancy and fully occupied layers share a common face and are respectively predominantly Ni- and Cr-centered. Interlayer interactions between these octahedra are predicted to be antiferromagnetic in nature owing to 90° d_σ–p_σ/p_π–d_π correlation superexchange. Despite the short (2.88 Å) separation between face-sharing octahedra, direct t_{2g}–t_{2g} interactions are weak, owing to the d^8 configuration of Ni(II), and may contribute to the lowering of the ordering temperature relative to Cr_3S_4. The existence of long-range magnetic order in $NiCr_2S_4$ contrasts with the behavior of VCr_2S_4, which is a spin-glass (4). We have suggested that spin-glass behavior is a consequence of magnetic frustration induced by next-nearest-neighbor V–Cr interlayer interactions. It would appear that in $NiCr_2S_4$ these interactions, which would be ferromagnetic, are sufficiently weak to result in a nonfrustrated system. The presence, at low temperatures, of diffuse scattering coincident with the magnetic reflection at $2\theta \approx 23°$ indicates that additional short-range magnetic correlations, possibly of the Ni–Ni intralayer type within the fully occupied layer, are present. It was not possible to separate the Bragg and diffuse scattering contributions to the intensity in this region with any degree of reliability and consequently, a correlation length could not be extracted from the data.

The ordered moments associated with cations at both crystallographic sites are considerably reduced from spin-only values: $\mu([M])$ to ca. 50% of the spin-only value for

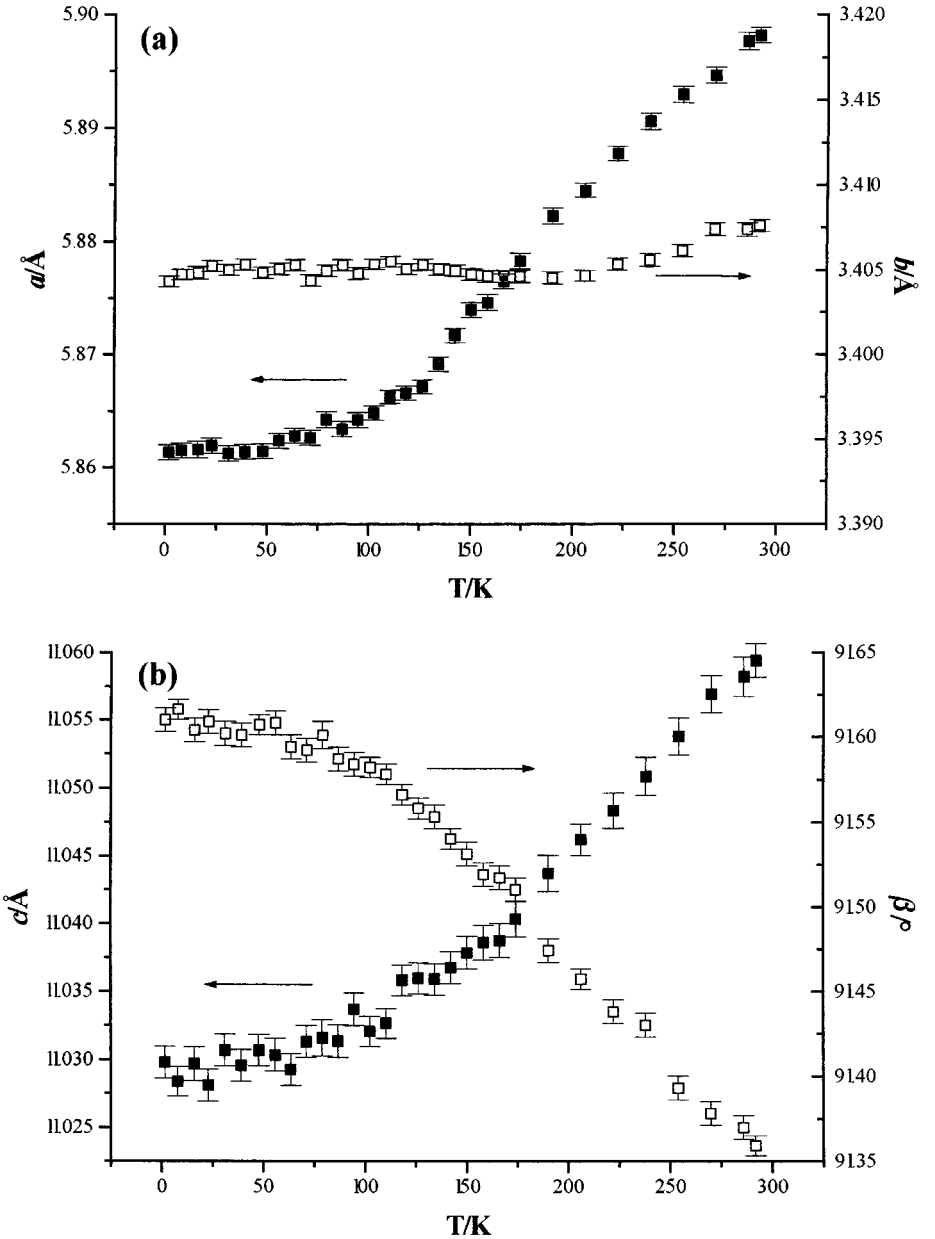

FIG. 8. Temperature dependence of the monoclinic unit cell parameters of $NiCr_2S_4$: (a) a and b parameters; (b) c and β parameters.

Cr(III) and $\mu((M))$ to ca. 70% of that expected for Ni(II). These reductions are to be expected, as the appreciable covalency of the metal–sulfur bonds will cause a transfer of spin away from the cations. Andron and Bertaut (10), using formulae derived from the work of Hubbard and Marshall (25), estimated covalency parameters of 10% for Ni^{2+} and 7.5% for Cr^{3+} assuming that the structure was of the normal type. A similar calculation using the moments derived here yields values of 10.7% (Ni^{2+}) and 12% (Cr^{3+}). Although these are consistent with values obtained for binary chalcogenides (26, 27), their significance is questionable, as they are derived from average moments at each of the sites. It has been suggested (11) that the unusual shape of the susceptibility curve results from competing exchange interactions of opposite sign. The neutron data presented here may be correlated with features of this curve. Neutron data unambiguously show that on cooling, long-range magnetic order is established at 180 K. This temperature corresponds to that at which the susceptibility begins to decrease. Below this temperature, the ordered moments at both sites continue to increase (Fig. 9) and the susceptibility falls further. At ca. 100 K, $\mu([M])$ reaches a saturation value, whereas $\mu((M))$ continues to increase. This growth of $\mu((M))$ may be correlated with the increase in susceptibility below

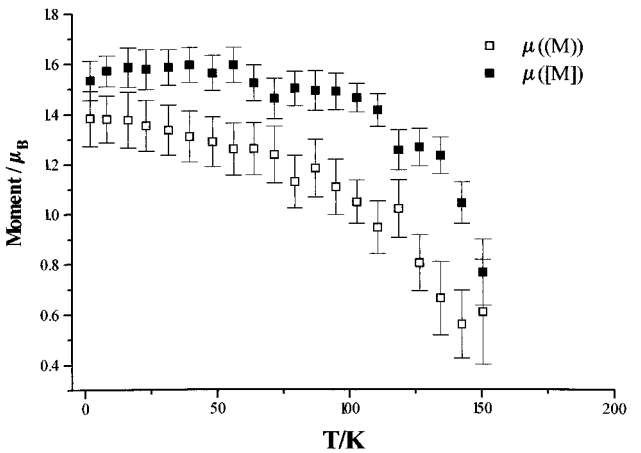

FIG. 9. Temperature dependence of the ordered moments associated with cations at sites in the vacancy (M) and fully occupied [M] layers in $NiCr_2S_4$.

100 K, which suggests that some small spontaneous magnetization remains in the complex magnetically ordered state.

Although some caution must be exercised in interpreting resistivity data obtained on sintered pellets, owing to contributions from grain boundaries, the temperature dependence of the electrical resistivity indicates that $NiCr_2S_4$ is a low-activation-energy semiconductor. Activation energies derived from a simple activated conduction plot are similar to those previously obtained for Cr_3S_4-type phases (8, 9). However, the material clearly lies close to the metal–insulator divide and data suggest that a further electronic transition may occur at higher temperatures (> 300 K). Magnetic ordering is accompanied by a decrease in the activation energy for electron transport, suggesting that spin-disorder scattering of the charge carriers is an appreciable contributor to the electrical resistivity.

In conclusion, it has been demonstrated that $NiCr_2S_4$ adopts a structure which is close to that expected for the normal structure type and orders magnetically at 180 K. The complex magnetic susceptibility may be accounted for by the different temperature dependence of the moments at the two crystallographic sites. The onset of magnetic order is accompanied by a lowering of the activation energy for electron transport.

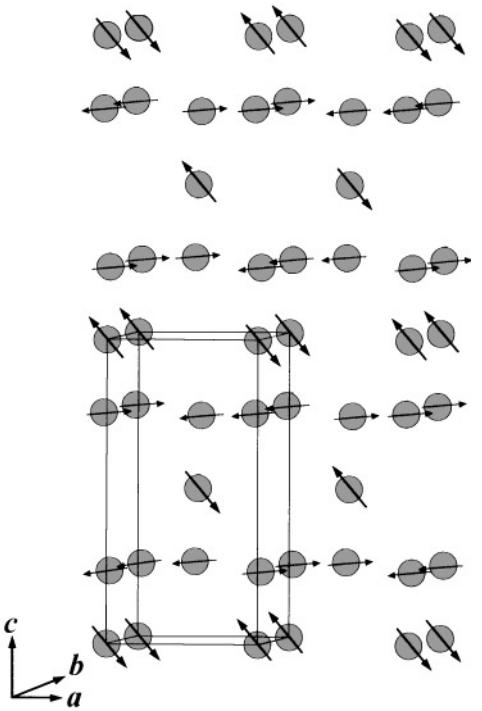

FIG. 10. A representation of the magnetic structure of $NiCr_2S_4$. Diamagnetic ions are omitted for clarity. Heavy arrows represent moments in the vacancy layer and lighter arrows represent moments in the fully occupied layer. The crystallographic unit cell is outlined.

ACKNOWLEDGMENTS

Financial support from the EPSRC (Grants GR/J36075 and GR/J34231) and The Royal Society is gratefully acknowledged. We wish to thank Dr. A. M. Chippindale, University of Oxford, for assistance with the energy-dispersive X-ray microanalysis measurements. D.C.C. thanks Heriot-Watt University for a studentship.

REFERENCES

1. F. Hulliger, *Struct. Bonding* **4,** 83 (1968).
2. A. Wold and K. Dwight, *in* "Solid State Chemistry: Synthesis, Structure and Properties of Selected Oxides and Sulphides," Chap. 11. Chapman and Hall, New York, 1993.
3. D. C. Colgan and A. V. Powell, *J. Mater. Chem.* **6,** 1579 (1996).
4. A. V. Powell and S. Oestreich, *J. Mater. Chem.* **6,** 807 (1996).
5. A. V. Powell and D. C. Colgan, *Mater. Sci. Forum* **228,** 831 (1996).
6. A. V. Powell and D. C. Colgan. *J. Mater. Chem.*, in press.
7. F. Jellinek, *Acta Crystallogr.* **10,** 620 (1957).
8. R. J. Bouchard and A. Wold, *J. Phys. Chem. Solids* **27,** 591 (1966).
9. S. L. Holt, R. J. Bouchard, and A. Wold, *J. Phys. Chem. Solids* **27,** 755 (1966).
10. B. Andron and E. F. Bertaut, *J. Phys.* (*Paris*) **27,** 619 (1966).
11. B. L. Morris, P. Russo, and A. Wold, *J. Phys. Chem. Solids* **31,** 635 (1970).
12. R. E. Tressler and V. S. Stubican, *J. Am. Ceram. Soc.* **51,** 391 (1967).
13. E. Whipple and A. Wold, *J. Inorg. Nucl. Chem.* **24,** 23 (1962).
14. A. C. Larson and R. B. von Dreele, "General Structure Analysis System," Los Alamos Laboratory, 1994. [Report LAUR 85-748]
15. P. J. Brown, *in* "International Tables for Crystallography" (A. J. C. Wilson, Ed.), Vol. C, Chap. 4. Kluwer, Dordrecht, 1992.
16. R. D. Shannon, *Acta Crystallogr., Sect. A* **32,** 751 (1976).
17. A. Hayashi, Y. Ueda, K. Kosuge, H. Murata, H. Asano, N. Watanabe, and F. Izumi, *J. Solid State Chem.* **71,** 237 (1987).
18. J. M. Newsam and Y. Endoh, *J. Phys. Chem. Solids* **48,** 607 (1987).
19. A. Hayashi, Y. Ueda, K. Kosuge, H. Murata, H. Asano, N. Watanabe, and F. Izumi, *J. Solid State Chem.* **67,** 346 (1987).
20. J. B. Goodenough, "Magnetism and the Chemical Bond," Chap. I. Wiley, New York, 1963.

21. D. Babot, M. Chevreton, J. L. Buevoz, R. Langier, B. Lambert-Andron, and M. Wintenberger, *Solid State Commun.* **30,** 253 (1979).
22. E. F. Bertaut, G. Roult, R. Aleonard, R. Pauthenet, M. Chevreton, and R. Jansen, *J. Phys.* (*Paris*) **25,** 582 (1964).
23. J. B. Goodenough, "Magnetism and the Chemical Bond," Chap. III. Wiley, New York, 1963.
24. J. Kanamori, *J. Phys. Chem. Solids* **10,** 87 (1959).
25. J. Hubbard and W. Marshall, *Proc. Phys. Soc.* **86,** 561 (1965).
26. B. E. F. Fender, A. J. Jacobson, and F. A. Wedgwood, *J. Chem. Phys.* **48,** 990 (1968).
27. A. J. Jacobson and B. E. F. Fender, *J. Chem. Phys.* **52,** 4563 (1970).